X-641-70-13
PREPRINT

THE CONTRIBUTION OF ATMOSPHERIC AEROSOLS TO THE MARTIAN OPPOSITION EFFECT

JAYLEE M. MEAD

JANUARY 1970

GSFC
GODDARD SPACE FLIGHT CENTER
GREENBELT, MARYLAND

X-641-70-13

THE CONTRIBUTION OF ATMOSPHERIC AEROSOLS TO THE MARTIAN OPPOSITION EFFECT

Jaylee M. Mead

Laboratory for Space Physics

January 1970

Submitted to Icarus

GODDARD SPACE FLIGHT CENTER
Greenbelt, Maryland

ABSTRACT

The Mie theory is used to compute the integrated scattering intensities for submicron aerosol particles with various indices of refraction and several size distributions in an effort to determine if the presence of atmospheric aerosols can account for the Martian opposition effect, as observed by O'Leary in 1967. This non-linear surge in brightness, as the planet approaches a phase angle of 0°, is reported to be much more pronounced in the ultraviolet than in the infrared.

The calculations show that neither substances having a refractive index $\underline{n}$ between 1.20 and 1.50, which include ice, water, and solid CO_2, nor highly absorbing materials, such as limonite, can produce the opposition effect. On the other hand, aerosols having $\underline{n} > 1.50$ with little or no absorption, such as meteoric particles or suspended surface dust composed of semi-transparent minerals, do exhibit a definite increase in reflectivity at small phase angles.

By introducing an assumed surface function, which is added to the contribution by aerosols with $\underline{n} = 1.75$, a model is obtained which compares reasonably well with the observations. A similar fit was obtained for $\underline{n} = 1.55$ and could probably be obtained for any real index between 1.55 and 1.75. This range includes most semi-transparent minerals, thus making them good candidates for producing the opposition effect.

This study demonstrates that the presence of a small amount of atmospheric aerosols, with the proper index of refraction, could provide the observed increased opposition effect for Mars in the ultraviolet, where the albedo is very low, but at the same time make a negligible contribution in the infrared, where the surface albedo is high.

THE CONTRIBUTION OF ATMOSPHERIC AEROSOLS TO THE MARTIAN OPPOSITION EFFECT

Jaylee M. Mead
Laboratory for Space Physics
NASA Goddard Space Flight Center
Greenbelt, Maryland 20771

I. Introduction

Observations of Mars made by O'Leary (1967a,b) during the 1967 opposition show an "opposition effect", i.e., a non-linear surge in brightness as the planet approaches 0° phase angle (the angle α at the planet between the directions to the sun and to the observer). Fig. 1 is taken from O'Leary and Rea (1968) and shows the Martian opposition effect in six colors: U, B, V, R, I, and I'. The observations, made at phase angles of 1.2° to 8°, are indicated by solid lines. Each curve was determined by deriving the best curve through the observed data points and fitting this curve between $\alpha = 12^\circ$ and 16° (depending upon the wavelength) to the known linear phase function reported for $\alpha \gtrsim 10^\circ$ (de Vaucouleurs, 1964). Note that the magnitude scales for the U and B curves at the top of Fig. 1 are compressed by a factor of two compared to the other colors shown; the opposition effect for U and B is therefore greater than a first glance at these plots suggests.

In Fig. 2 we plot the reflectivities from Fig. 1, as adjusted for the color of the sun, on a single continuous scale. On the right side of the figure, reflectivity p is shown on a logarithmic scale; its equivalent magnitude, given by $m = -2.5 \log_{10} p$, is shown on the

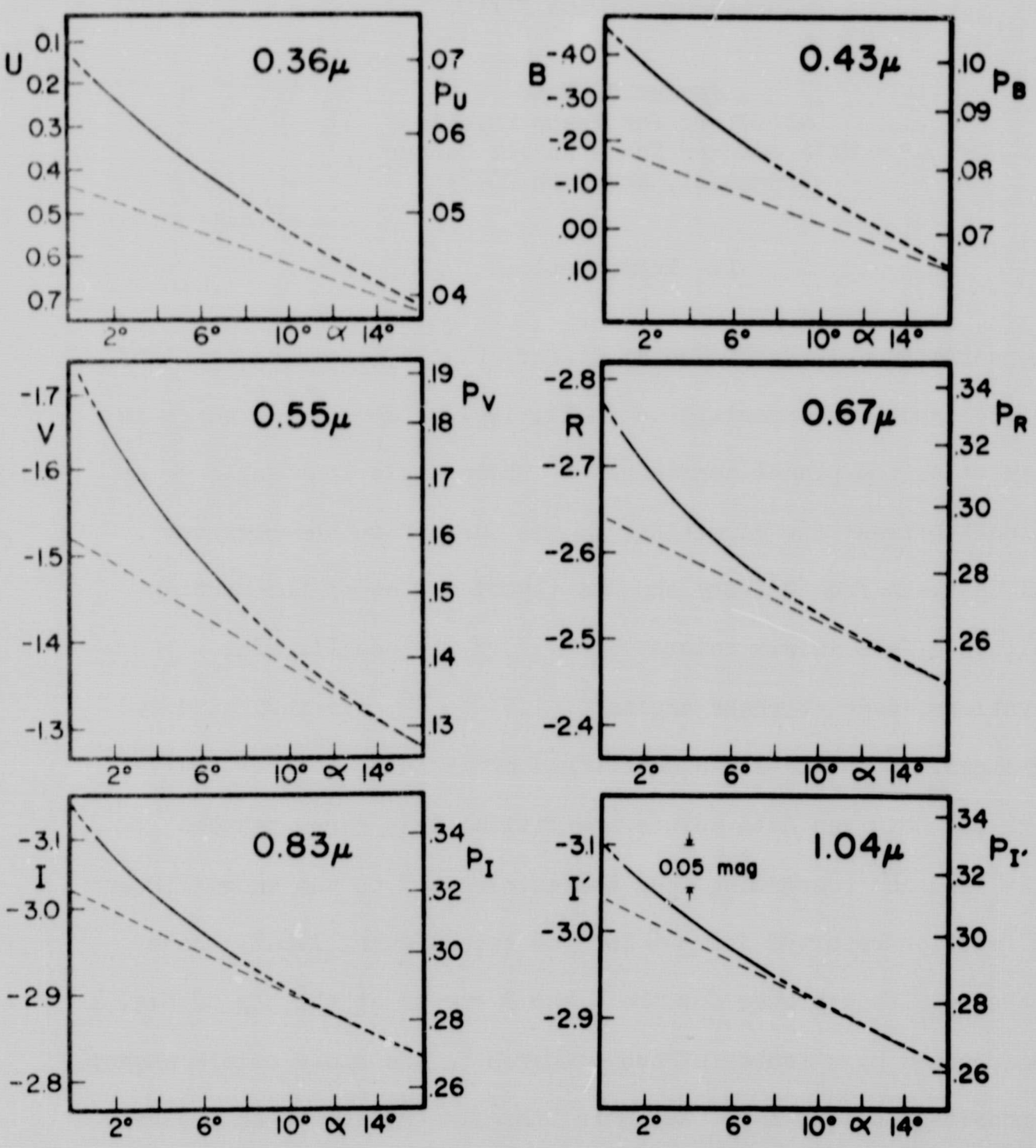

Figure 1. The Martian opposition effect in six colors fitted to the linear phase functions for $\alpha \gtrsim 10^{\circ}$ reported by de Vaucouleurs (1964). Values for the absolute magnitude are the ordinates on the left sides of the figures, and reflectivities normalized to geometric albedos are the ordinates on the right sides of the figures. (O'Leary and Rea, 1968).

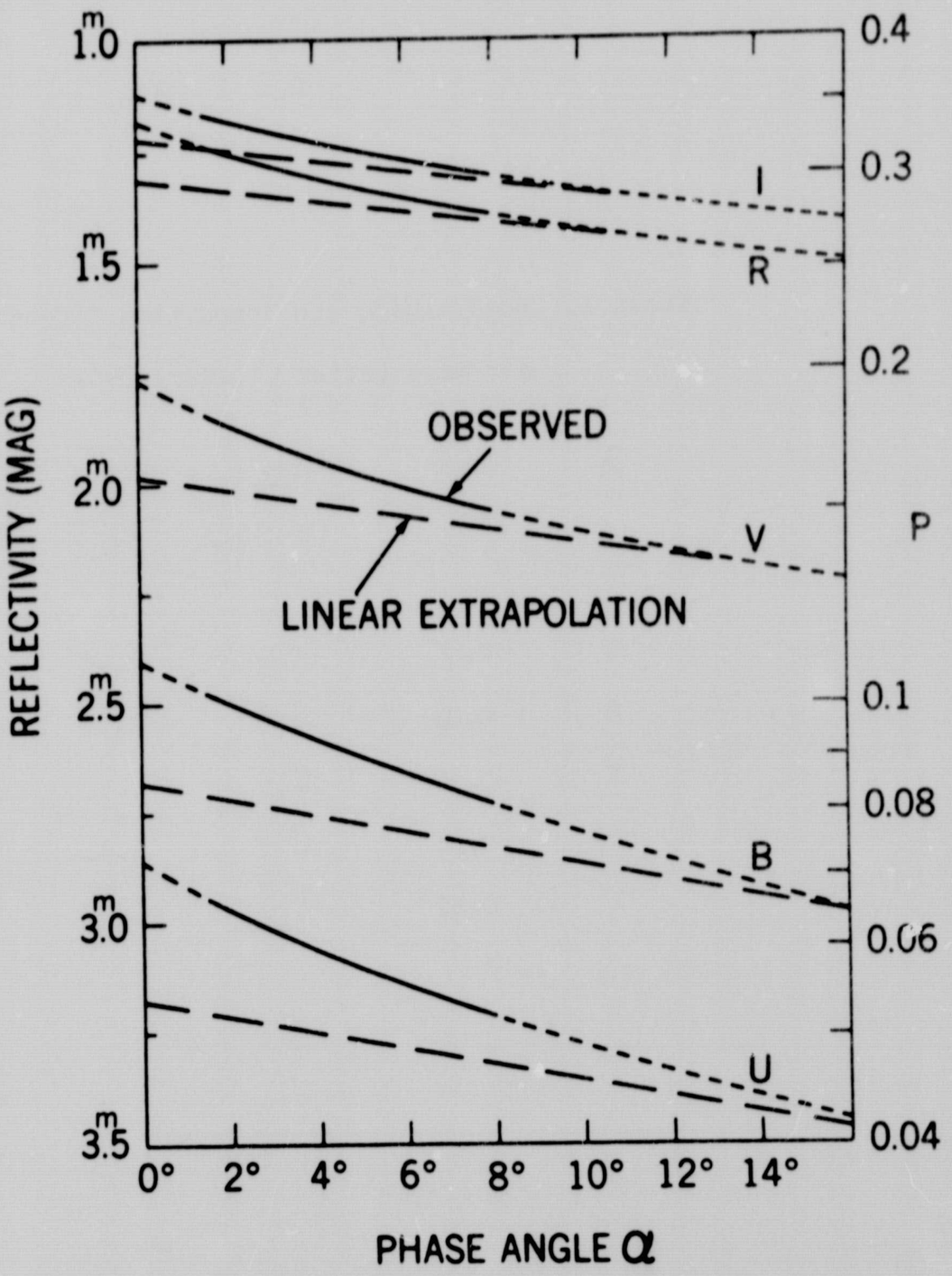

Figure 2. The Martian opposition effect, after O'Leary and Rea (1968), adjusted for the color of the sun. Reflectivity is shown on a logarithmic scale on the right and on an equivalent magnitude scale on the left.

Table I. Bond Albedo and Opposition Effect for Mars (after O'Leary, 1967b)

λ	Bond Albedo	Δ m (0 - 16°)	$\frac{B_{0°}}{B_{16°}}$
U	0.05	$0^m.59$	1.72
B	0.08	$0^m.56$	1.68
V	0.17	$0^m.45$	1.52
R	0.38	$0^m.32$	1.34
I	0.42	$0^m.29$	1.30

left. The reflectivity scale has a range of 2.5 magnitudes, or a factor of 10. As O'Leary and Rea pointed out, the opposition effect is much more pronounced at shorter wavelengths than at longer wavelengths, as evidenced by the fact that the U and B observations depart much more from the linear extrapolation than do the curves at R and I. The reflectivity, or albedo, on the other hand, is much greater at longer wavelengths than at shorter ones.

Table I expresses these concepts quantitatively. Note that the Bond albedo of Mars is only 5% in U, whereas it is 42% in I; yet the brightness increases by 72% from 16° to 0° phase angle in the U, but only 30% in the I.

This increased opposition effect in the blue and ultraviolet could be primarily a surface effect in that the surface may have a much greater increase in reflectivity at shorter wavelengths; alternatively, it could be primarily due to light scattering in the atmosphere, as suggested by O'Leary (1967a).

Rayleigh scattering by molecules and by particles small compared to the wavelength of observation does not provide a sudden increase of brightness near 0° phase angle. Therefore, if the effect is primarily atmospheric, particles of larger size must be responsible.

Because of the low albedo in the U, a small brightness contribution by atmospheric aerosols will have a comparatively large effect; in the I, where the surface is much brighter, a small brightness contribution by aerosols will cause little or no change in the total brightness.

The purpose of this study is to investigate the contribution which atmospheric aerosols might make to the Martian opposition effect, under the assumption that the increased enhancement in the shorter wavelengths, where the surface albedo is low, is primarily an atmospheric effect rather than a surface effect. Here we define the term atmospheric aerosol as the particulate matter suspended in the planet's atmosphere.

The study is divided into four parts:

1. Calculations of scattering intensity near 0° phase angle (180° scattering angle) by single particles, using Mie scattering theory.
2. Calculations of integrated intensities obtained by summing over particle size distributions.
3. Development of a model which incorporates a surface photometric function plus an aerosol contribution, which is then compared with the observations.
4. Examination of possible sources of Martian atmospheric aerosols.

II. Light Scattering by Single Particles

The Mie scattering theory, which describes single scattering by spherical particles, was used to make light scattering calculations for substances such as ice, water, and solid CO_2, which have no significant absorption in the wavelength range under consideration. In addition, calculations were made for highly absorbing materials, such as limonite.

When unpolarized light of intensity I_o is incident upon a spherical aerosol particle of radius a, the intensity I of the radiation scattered in the direction θ and at a distance r from the particle is given by

$$I = \frac{I_o \lambda^2}{8 \pi^2 r^2} \left[i_1 (x, \tilde{n}, \theta) + i_2 (x, \tilde{n}, \theta) \right] \qquad (1)$$

where $x = 2\pi a/\lambda$ = size parameter;

$\theta = 180^\circ - \alpha$ = scattering angle (the angle between the direction of propagation of the incident wave and the scattered wave), where α is the phase angle;

$\tilde{n} = n - ik$ = complex index of refraction of scattering particle; $k = 0$, if non-absorbing; $k > 0$, if absorbing;

λ = wavelength of incident light in the surrounding medium.

Here i_1 and i_2 are the dimensionless intensity functions given by the Mie theory as described by van de Hulst (1957, p. 35). Note that the particle radius a and the wavelength λ enter these intensity functions only through the size parameter x.

Calculations were made for aerosols with $\underline{n}$ between 1.20 and 2.40 with no absorption ($\underline{k} = 0$), small absorption ($\underline{k} = 0.01$ and 0.03) and large absorption ($\underline{k} \geq 0.1$). Of special interest for studies of Mars are the results obtained for the following refractive indices: 1.31 (ice), 1.33 (water), 1.35 (solid CO_2: Egan and Spagnolo, 1969), 2.23 - 0.669$\underline{i}$ (limonite at $\underline{\lambda} = 0.365\mu$: Egan and Becker, 1969). The maximum size parameter examined was $\underline{x} = 83$; however, the current study has been restricted to submicron particles. Phase angles as large as 60° have been considered, although the maximum phase angle at which Mars is observable from earth is ~47°.

Since the O'Leary-Rea observations begin to depart from linearity in the U and B at around 15° phase angle (cf. Fig. 1), the calculated scattering intensities were normalized by dividing each value by the average intensity at phase angles from 12° – 18°. These intensity ratios, converted to a magnitude scale, are shown schematically in Fig. 3, for $\underline{n} = 1.35$ with no absorption, using the code given in Table II. The size parameter $\underline{x}$ is given in the first column on the left. The radius scales corresponding to the wavelengths 0.36μ(U), 0.55μ(V), and 0.83μ(I) are shown in the next three columns. Adjacent bars of the same kind, either vertical or horizontal, have been connected. Thus, in regions of continuous solid vertical bars (such as for $6° < \underline{\alpha} < 12°$ and $17 < \underline{x} < 20$), the scattering intensity is at least $1^m.25$ <u>brighter</u> than the average scattering intensity from 12° to 18° phase angle for that size

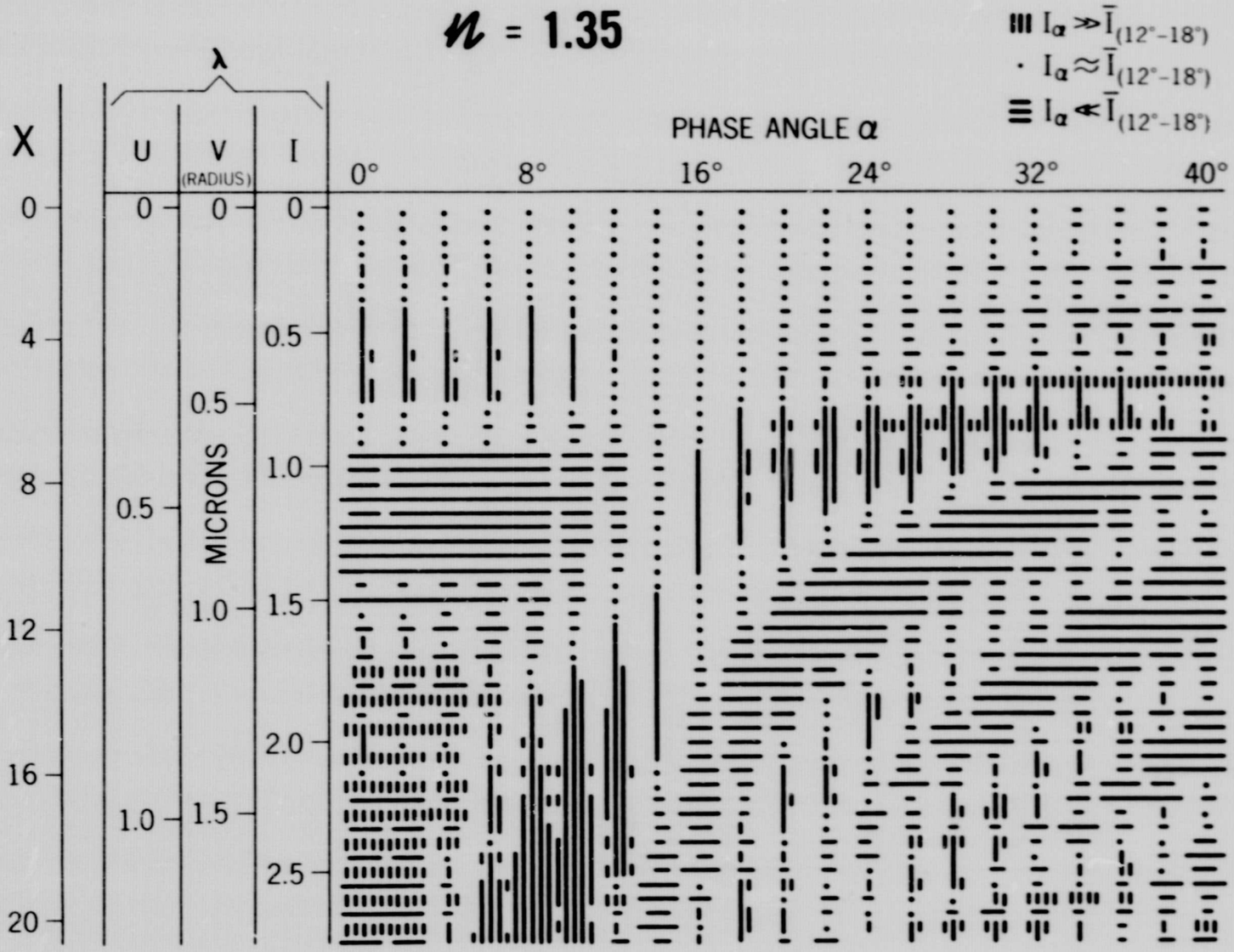

Figure 3. Schematic diagram of the scattering intensity for Mie aerosols of refractive index 1.35, normalized to the average intensity for $12° \leq \alpha \leq 18°$. The first column gives the Mie size parameter, $x = 2\pi a/\lambda$, where a = particle radius as given in the next three columns for wavelengths 0.36 (U), 0.55 (V), and 0.83 (I) micron. See Table II for code used to construct diagram.

Table II. Code Used for Schematic Scattering Intensity Diagrams Shown in Fig. 3-6.

Code	Magnitudes $m(\alpha) - m_{average}(12^{\circ} - 18^{\circ})$
|||||	$\leq -1.^{m}25$
||||	-1.00
|||	-0.75
||	-0.50
|	-0.25
.	0.0
-	+0.25
--	+0.50
---	+0.75
----	+1.00
-----	$\geq$ +1.25

parameter. A dot indicates that the scattering intensity is within $\pm 0^{m}.125$ of the $12^{\circ} - 18^{\circ}$ average. A region of solid horizontal bars (such as for $0^{\circ} < \alpha < 8^{\circ}$ and $7 < x < 10$) shows that the scattering intensity is at least $1^{m}.25$ or more fainter than the average scattering intensity from $12^{\circ} - 18^{\circ}$.

The usefulness of this display lies in allowing us to observe how the scattering intensity for a given particle radius and wavelength varies with phase angle, and thus to see what particle sizes show an increase in intensity, or brightness, near small phase angles, and which do not. As noted earlier, the Martian opposition effect is observed to depart from linearity around 15° phase angle in the U and B; therefore, we will be looking for particle sizes which give an enhancement at small angles---that is, lots of vertical lines near 0° phase angle.

If we consider for the moment only submicron particles, and if we look in Fig. 3 for the radii which will give a brightness increase at small phase angles, we see a small enhancement by particles in the U having radii between about 0.2 and 0.35 micron. (This would correspond to 0.3 and 0.5 micron particles in the V, and 0.4 to 0.7 micron radii in I). This is only about $\frac{1}{4}$ magnitude brighter than the average intensity around 15°, as indicated by the low density of vertical lines (cf. Table II.) Radii between 0.3 and 0.45 micron in U show an enhancement at larger (not smaller) phase angles ($18^{\circ} \leq \alpha \leq 40^{\circ}$); while radii between 0.4 and 0.6 micron exhibit an anti-opposition effect at $0^{\circ} \leq \alpha \leq 12^{\circ}$, as evidenced by the large number of horizontal lines.

Further down the diagram, at larger radii, where there is a spotty positive effect, the solid-line enhancement occurs for phase angles of 6° - 12°, as noted earlier, which is not what the Mars observations show. Thus it does not appear that submicron spherical particles with refractive index 1.35 are good candidates for producing the opposition effect. Similar displays for refractive indices from 1.20 to 1.50 all produce only small variations of the basic picture seen here.

As mentioned earlier, the refractive index of 1.35, for which the Fig. 3 computations were made, is of particular interest for studies of Mars since it is the only measurement found in the literature for solid CO_2 in the ultraviolet. These measurements, which were made by Egan and Spagnolo (1969) for bulk CO_2, cover the wavelength range 0.35 to 1.0 micron and show little or no wavelength dependence. The absorption coefficient $\underline{k}$ reported by these authors is very small in this wavelength range and can be neglected in our calculations. Thin-film measurements of the refractive index for CO_2 cryodeposits by Tempelmeyer and Mills (1968) show slightly higher values for the real part of the refractive index and a variation with wavelength. They obtained a value of $\underline{n} = 1.455$ at $\underline{\lambda} = 0.6\mu$, the shortest wavelength at which their measurements were reported; however, the slope of their curve at this point suggests that the index might be increasing toward shorter wavelengths. Egan and Spagnolo (1969) have suggested that the discrepancy in these measurements may be due to the difference in temperature (and therefore density) of the

samples (77°K for Tempelmeyer and Mills vs. 195°K for Egan and Spagnolo); alternatively, surface or body scattering could reduce the observed Brewster angle, thus resulting in a slightly lower real portion of the index of refraction. Additional measurements of the refractive index of solid CO_2 over this range of temperature are desirable.

Fig. 4 gives a similar plot of scattering intensities for a highly absorbing material, limonite, using the complex refractive index in the ultraviolet as measured by Egan and Becker (1969). Here there is almost no change in scattering intensity with phase angle for a given particle radius. Thus aerosols of limonite, or of any other highly absorbing substance, could not produce an opposition effect. Similar results were found for all absorbing refractive indices where $k \geq 0.1$.

Fig. 5 shows scattering intensities for $n = 1.55$. Here the different picture looks considerably/from either of the previous displays. There is a strong continuous enhancement from 0° - 10° phase angle, with very small contributions at larger phase angles, for radii in the U ranging from around 0.2 to 0.7 micron. We can see that this same particle size range would show a smaller enhancement in the V and much less in the I.

Indications of an even more significant opposition effect are exhibited by calculations for aerosols having refractive index 1.75, as shown in Fig. 6. This display is typical for real indices of refraction from 1.60 to 2.00. From 2.00 to 2.40 the effect gradually decreases.

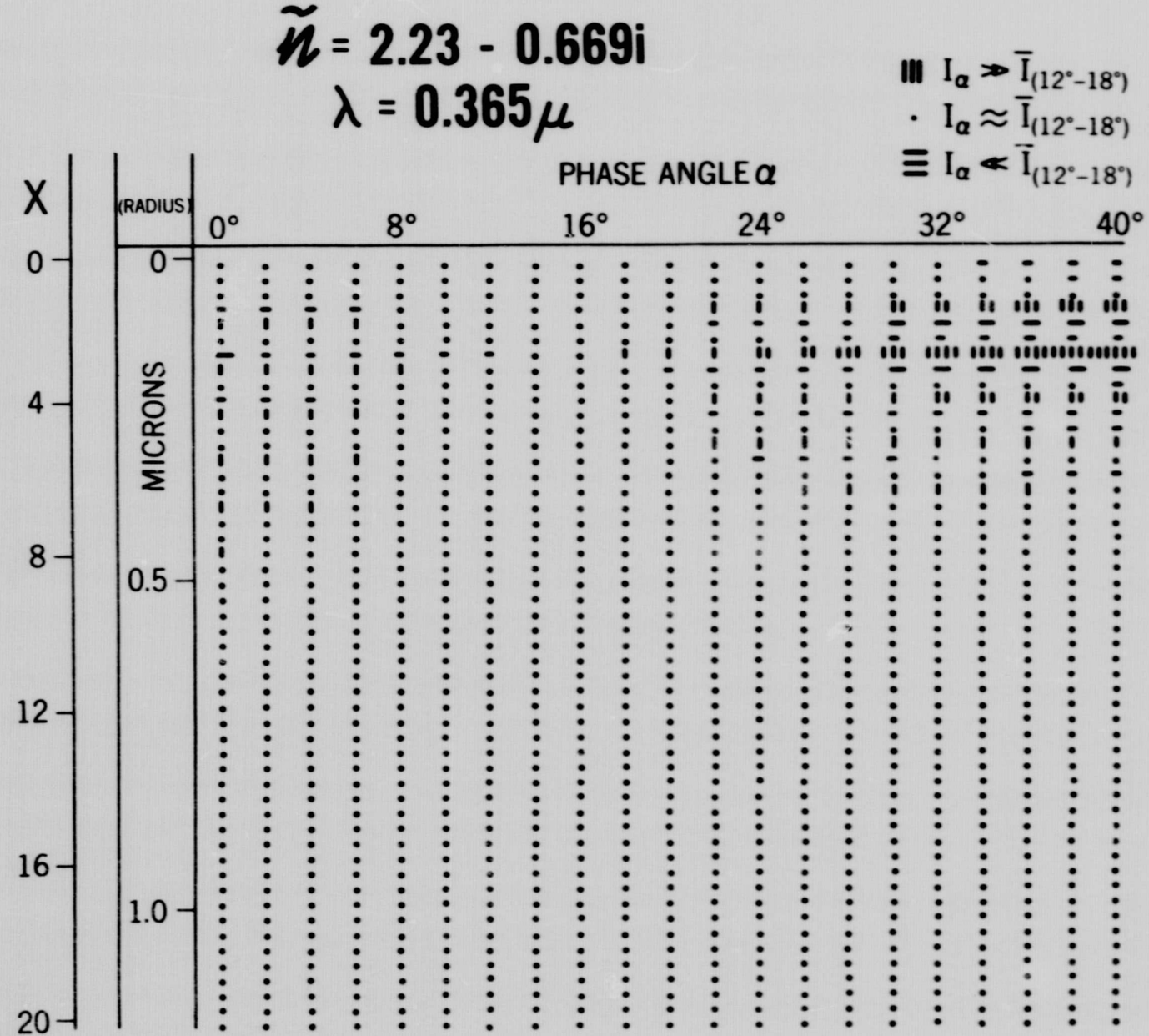

Figure 4. Same as Figure 3, except $\tilde{n}$ = 2.23 - 0.669i, λ = 0.365 micron.

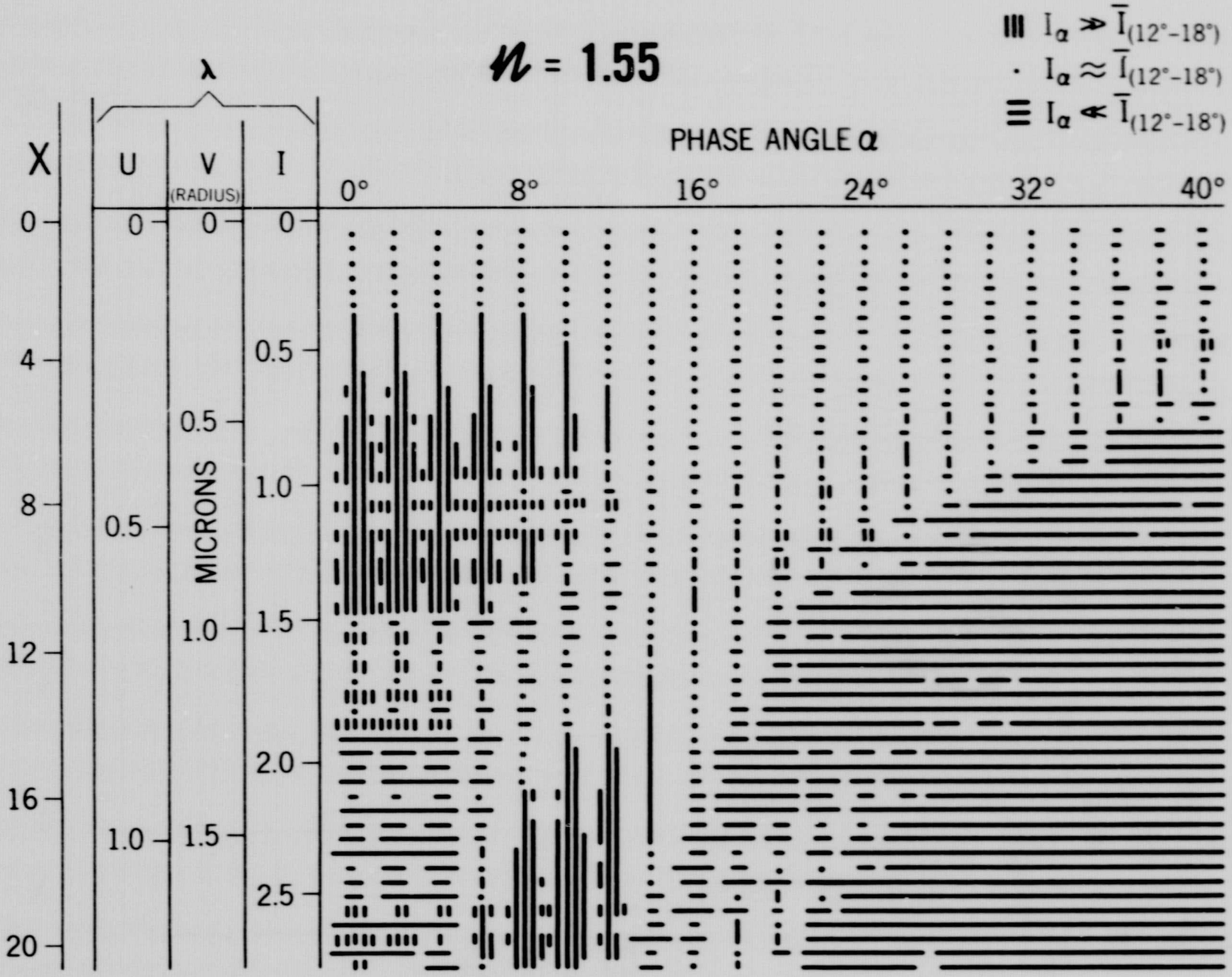

Figure 5. Same as Figure 3, except n = 1.55.

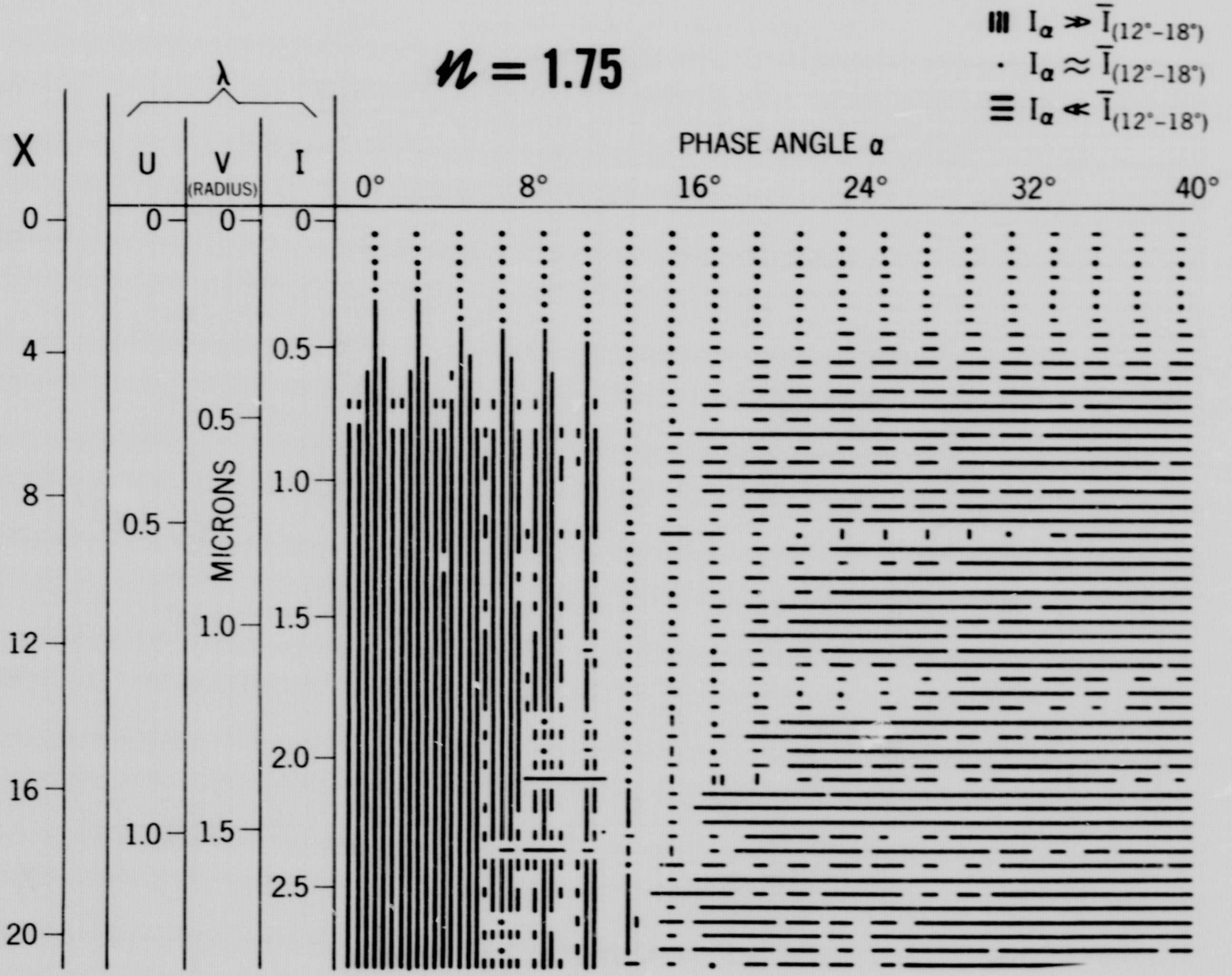

Figure 6. Same as Figure 3, except n = 1.75.

III. Integrated Intensities for Particle Size Distributions

Fig. 7 shows five particle size distributions $N(a)$, which are typical of those used in the Mie calculations to obtain integrated scattering intensities. Although calculations were made for distributions over particle radii ranging up to 4 microns, for this study we have considered only submicron particles. Two types of distributions have been used, as illustrated in Fig. 7: negative exponentials and skewed gaussian-type distributions. Distribution E-1 emphasizes very small particles by including primarily radii less than 0.4 micron. E-2 is much broader, thus including larger particles. The three skewed gaussian-type distributions shown in Fig. 7 peak at 0.2, 0.4, and 0.6 micron.

Eq. (1) gives the intensity I of the light scattered by a single particle of radius a. For a particle size distribution where $N(a)da$ = number of particles between a and $a + da$, the integrated intensity I' is

$$I' = \frac{I_0 \lambda^2}{8\pi^2 r^2} \int_a \left[i_1(x, \tilde{n}, \theta) + i_2(x, \tilde{n}, \theta) \right] N(a)\, da \qquad (2)$$

This expression has been evaluated for various indices of refraction and particle size distributions, and plotted in terms of magnitudes, as shown in Fig. 8-10. Only a relative magnitude scale is given on these plots, because the absolute magnitude depends on the total aerosol number density, which is a free parameter in our calculation. The normalization which was made for the single particle schematic displays in Fig. 3-6 has not been used in these calculations of integrated intensity.

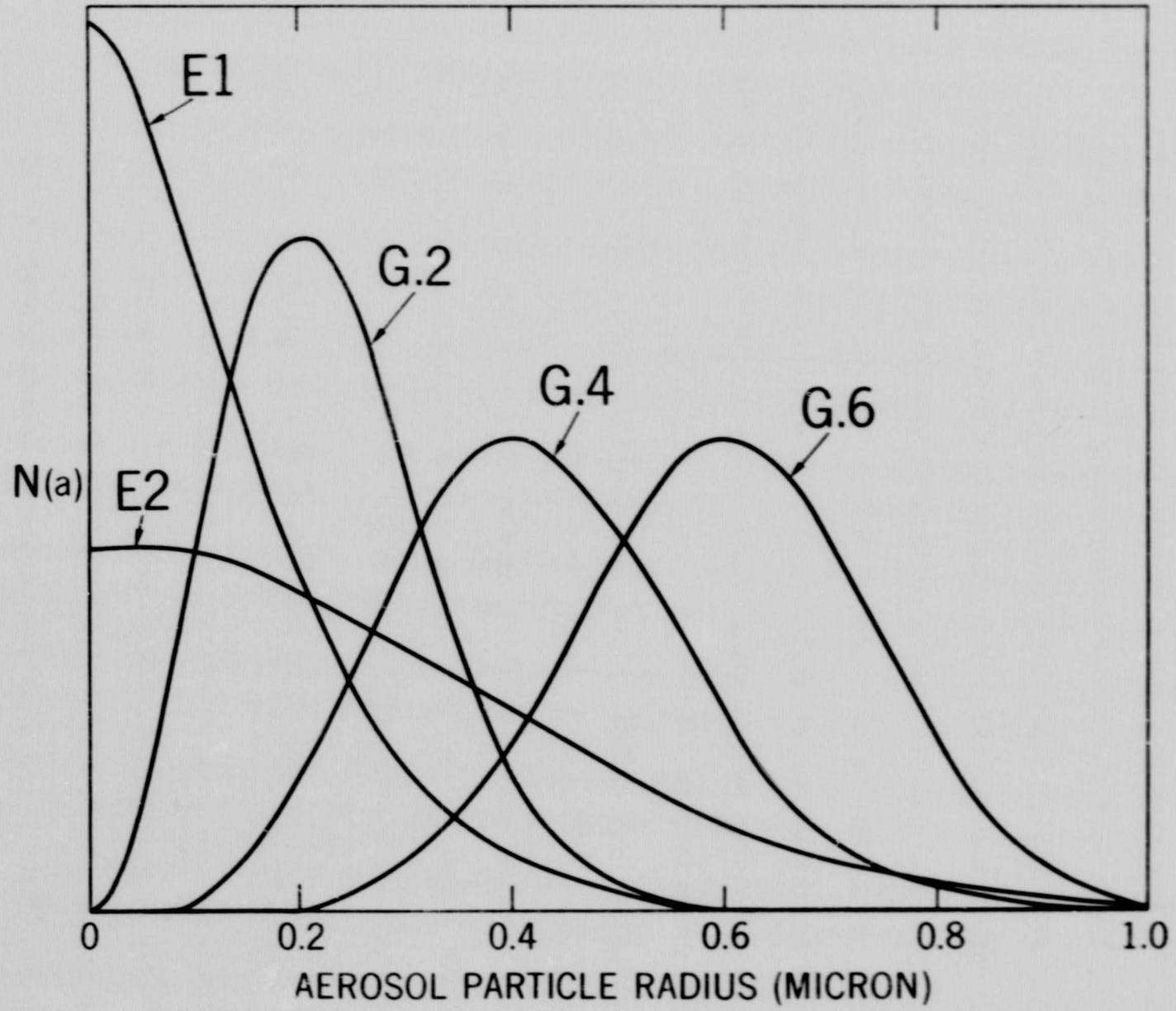

Figure 7. Typical particle size distributions used in calculations of integrated scattering intensities.

Fig. 8 shows the integrated intensities for $\underline{n} = 1.35$. Calculations are displayed for five wavelengths and two particle size distributions as a function of phase angle. From Fig. 3, the single-particle display for $\underline{n} = 1.35$, we recall that only a few very small particles showed a slight opposition enhancement, whereas particles of a little larger size showed an enhancement at larger phase angles. This behavior is reflected in the results obtained with Distribution E-1 of Fig. 8. When larger particles are weighted more heavily, as with Distribution G.6, the brightness curves peak at phase angles greater than 10°, as could be expected from examining the contributions from single particles.

Thus it appears that aerosols of refractive index 1.35 cannot produce the required opposition effect. Other distributions of larger-size particles were also incapable of simulating the observations. The same was generally true for all real refractive indices from 1.20 to 1.50.

Fig. 9 shows the integrated intensities for $\underline{n} = 1.55$. The same negative exponential and skewed gaussian-type distributions have been used here as in Fig. 8. As suggested by the single-particle display, there is a definite increase in the integrated intensity for both distributions from around 10° phase angle.

An even more impressive example of an opposition effect is seen in Fig. 10, where $\underline{n} = 1.75$. The increase in intensity from 15° to 0° in the U for Distribution G.4 is about 2.^{m}0, or about a factor of 6.

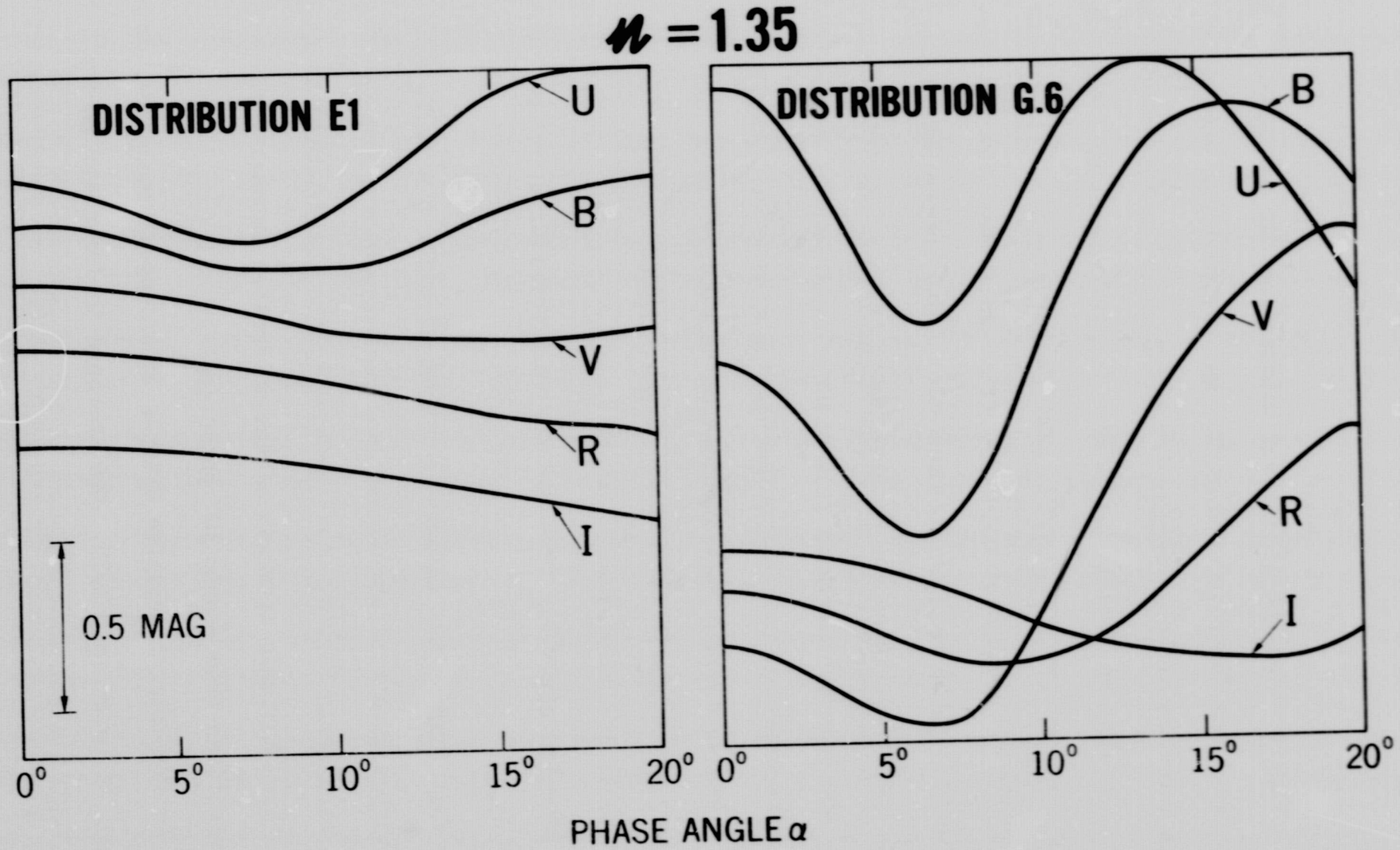

Figure 8. Integrated scattering intensities for aerosols of refractive index 1.35, as obtained with two particle size distributions. Intensity in magnitudes is plotted versus phase angle for the five wavelengths: 0.36 (U), 0.43 (B), 0.55 (V), 0.67 (R), and 0.83 (I) micron.

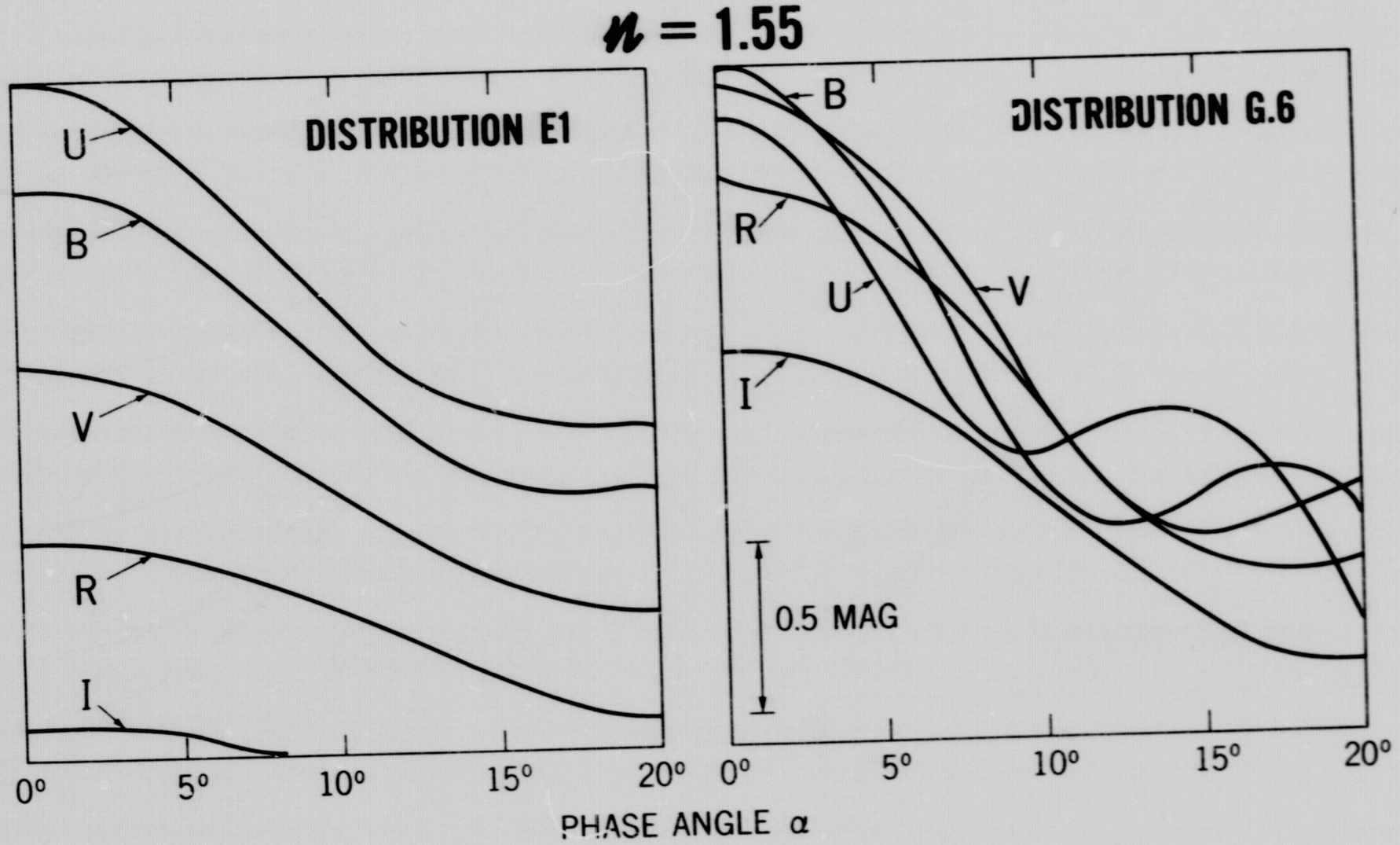

Figure 9. Same as Figure 8, except n = 1.55.

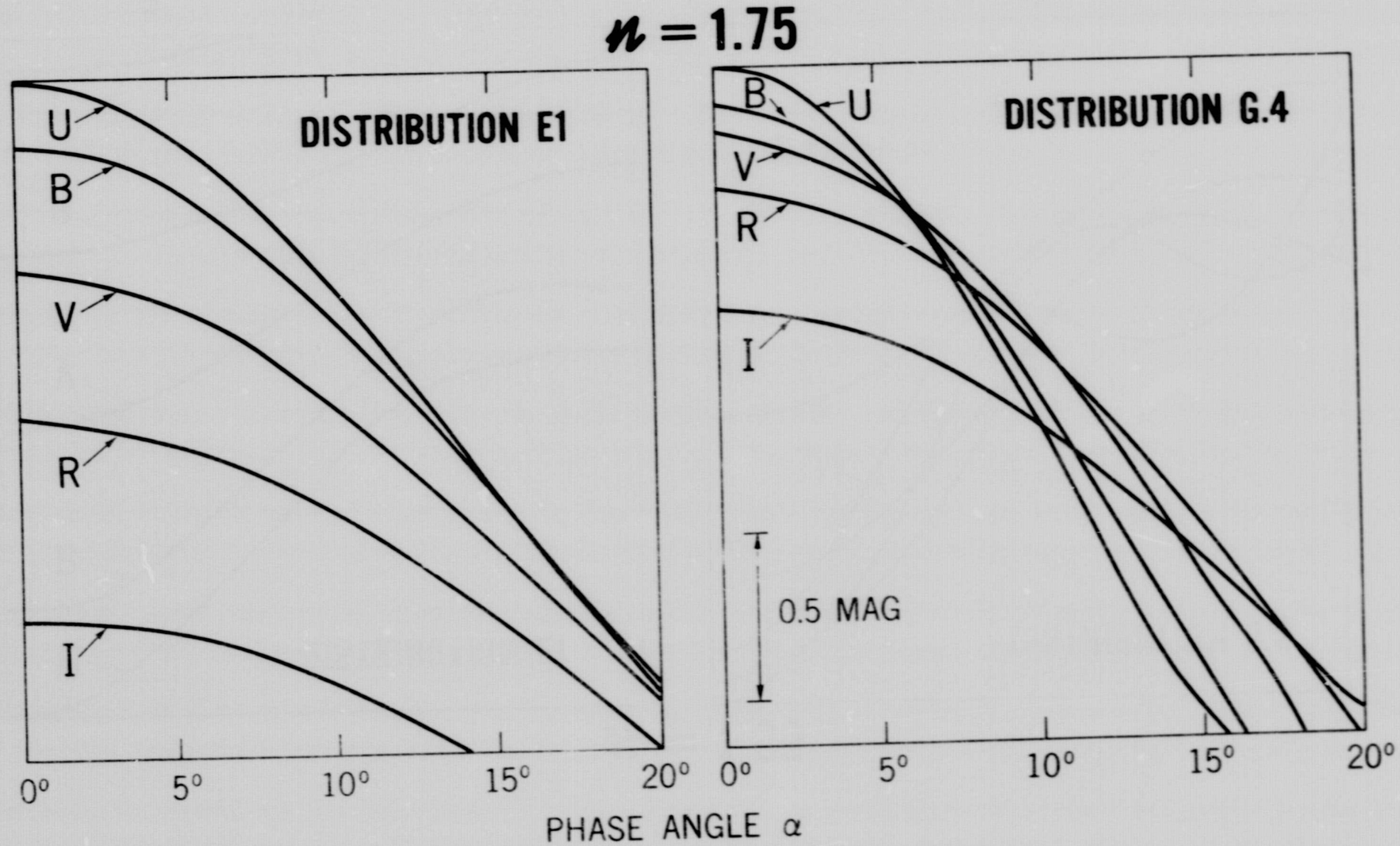

Figure 10. Same as Figure 8, except n = 1.75.

IV. Model of Surface Plus Aerosols and Comparison with Observations

Having found that refractive indices of 1.55 or greater could produce a significant enhancement in intensity at small phase angles, we next generated a model consisting of a surface brightness function plus a brightness contribution by atmospheric aerosols. At longer wavelengths, where the Martian albedo is higher and where surface markings are more clearly visible, it is reasonable to assume that the observed brightness comes almost entirely from the surface and that the brightness contribution by aerosols is negligible. As suggested by de Vaucouleurs (1968), we took the lunar photometric function developed by Hapke (1963) and modified it to fit the observed Martian brightness-phase curve at these longer wavelengths. We then assumed that the phase curve for the surface would have the same shape (when plotted on a magnitude scale) in all colors; only the albedo would change. This meant that in this model, the surface brightness would increase by 30% from 16° to 0° phase angle at all wavelengths. These assumed surface functions are shown as the thin lower curves for I, V, B and U in Fig. 11 (R has been omitted for simplicity).

The effect of the aerosols was then introduced. The upper heavy solid curves in Fig. 11 represent the calculated brightness of surface plus aerosols for refractive index 1.75 and a skewed gaussian-type particle distribution peaked at 0.4 micron (Distribution G.4) (cf. Fig. 10). At shorter wavelengths, where the albedo and surface contrast are greatly reduced, the atmospheric aerosols are seen to play a significant role.

The calculated phase curves are in reasonable agreement with the observations, shown as dashed lines. One should bear in mind, however, that there was a good deal of arbitrariness in obtaining this fit. It is by no means a unique solution to the problem. It does show, nonetheless, that the presence of a small amount of atmospheric aerosols, with the proper index of refraction, could provide the observed increased opposition effect for Mars in the ultraviolet, where the albedo is very low, but at the same time make a negligible contribution in the infrared, where the surface albedo is high.

Table III shows the reflectivities of the surface (p_s) and the aerosols (p_{ar}) for U, V and I at phase angles 0° and 16°, and the ratio of the aerosol brightness to the surface brightness, as obtained from this model. Note that p_{ar}/p_s reaches a maximum of 0.69 in the ultraviolet at opposition, but falls off rapidly both with increasing wavelength and increasing phase angle. Since p_{ar} is always less than 3% in this model, the atmosphere is optically thin at all wavelengths, and the assumption of single scattering is justified.

The reflectivities in Fig. 1, 2, and 11 and Table III have been normalized to the intensity of a Lambert disk I_L with the same radius as the planet, viewed at 0° phase angle, given by

$$I_L = I_0 A / \pi r^2 \qquad (3)$$

where A is the cross-sectional area of the planet and r is the distance

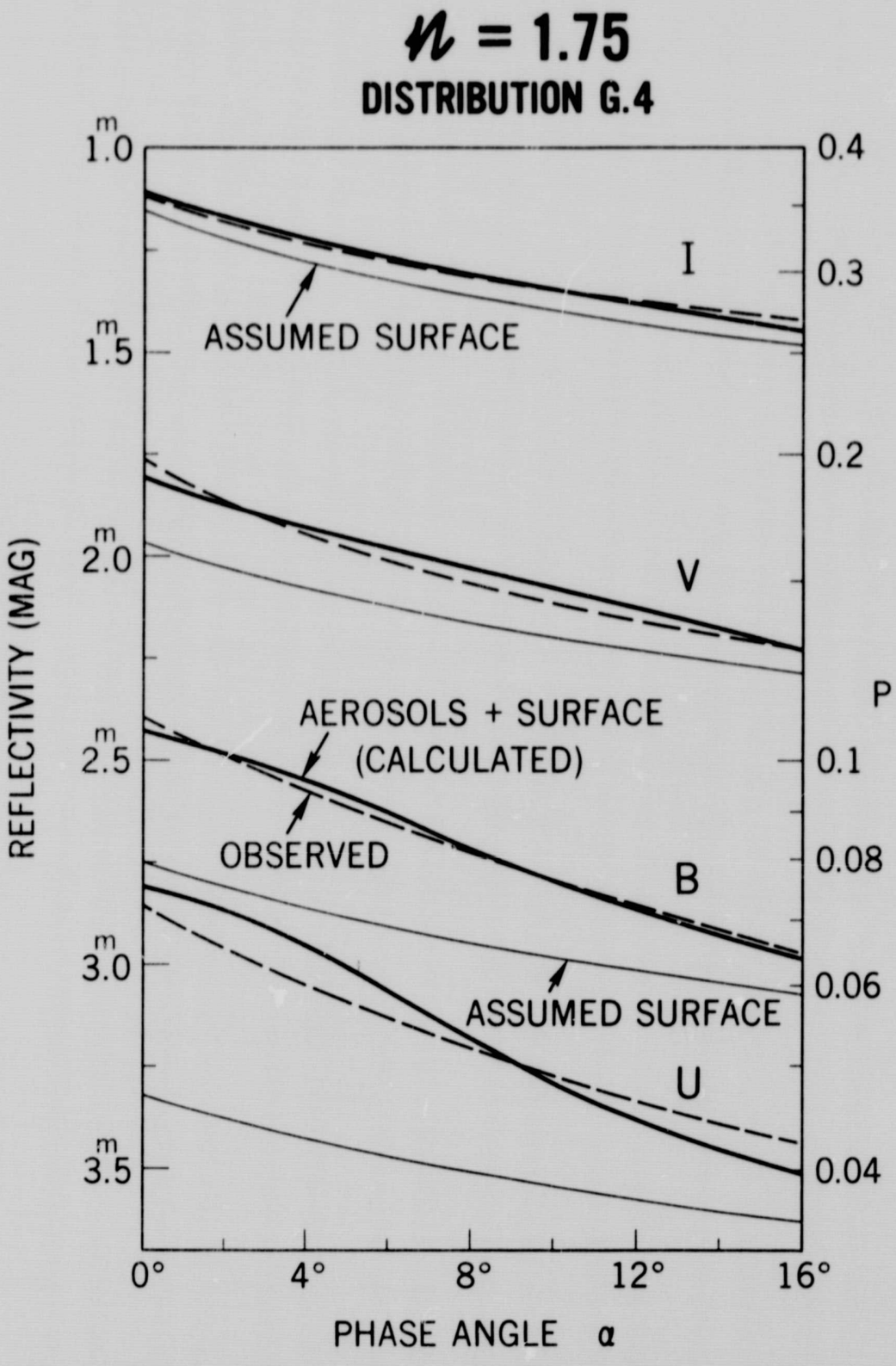

Figure 11. Comparison of model with Mars observations. For each wavelength, the thin lower curve is the assumed surface reflectivity, the heavy upper curve is the calculated brightness from the surface plus aerosols, and the broken curve is the Martian observational data.

Table III. Reflectivity of Surface and Aerosols, as Obtained with Model for $\underline{n} = 1.75$ and Distribution G.4

α	λ	p_s	p_{ar}	(p_s+p_{ar})	$\frac{p_{ar}}{p_s}$
	U	0.045	0.031	0.076	0.69
0°	V	0.162	0.026	0.188	0.16
	I	0.344	0.015	0.359	0.04
	U	0.035	0.005	0.040	0.14
16°	V	0.123	0.008	0.131	0.06
	I	0.260	0.008	0.268	0.03

to the observer. From Eq. (2) and (3) we computed that a columnar particle density of 0.9×10^6 aerosol particles/cm^2 was required to give the reflectivities of the aerosol layer shown in Table III. Assuming an average particle radius $\underline{a} = 0.4\mu$ (cf. Dist. G.4, Fig. 7) with a density of 2.5 gm/cm^3, a value typical of semi-transparent minerals (see next section), we find that the number of aerosols required in the above model corresponds to a columnar mass of 7×10^{-7} gm/cm^2.

This number can be compared with the columnar mass of the gaseous atmosphere on Mars, which is 19 gm/cm^2 for a surface pressure of 7 mb. The mass ratio of aerosols to gaseous atmosphere for our model is therefore 4×10^{-8}, thus demonstrating that only a very small amount of aerosols is needed to produce the observed opposition effect.

The only results of our model which are shown here (cf. Fig. 11 and Table III) are those for aerosols with refractive index 1.75. However, a reasonable fit to the observational data was also obtained with atmospheric particles of refractive index 1.55, and could probably be obtained with any real index between 1.55 and 1.75. Such a fit was not found for aerosols having refractive index of 1.50 or less.

V. Sources of Martian Atmospheric Aerosols

Several sources can account for the presence of aerosols in a planetary atmosphere: 1) *in situ* particle formation through condensation, photochemical reactions, and coagulation of the gaseous atmospheric constituents, 2) influx of meteoric particles, and 3) upsweeping of dust from the surface of the planet.

1. A few atmospheric aerosols which might be formed *in situ* have already been considered in the calculations for water, ice and solid CO_2 particles; they were found to be incapable of producing the observed opposition effect. However, measurements of Mariner 6 taken at 79°N latitude at the beginning of polar night indicate that conditions in the Martian atmosphere are favorable for the condensation of CO_2 at almost all altitudes; Mariner 7 measurements taken at 58°S in daytime and 38°N at night also show that CO_2 condensation is possible at altitudes above about 25 km (Kliore et al, 1969). Condensation of CO_2 is predicted for atmospheric temperatures below 150°K. The only available refractive indices for solid CO_2 at $\lambda < 0.6\mu$, as pointed out earlier, were made at $T = 195°K$ (Egan and Spagnolo, 1969). Should the refractive index be significantly higher at $T < 150°K$, the above conclusions with regard to solid CO_2 aerosols would need revision. It is highly desirable, therefore, to have additional measurements of the refractive index of solid CO_2 at $T < 150°K$, $\lambda < 0.6\mu$. Current estimates of the concentration of CO_2 on Mars range from 60 to

100 percent (Kliore et al, 1969); therefore, the role of other gaseous atmospheric constituents should not be ignored as possible sources of atmospheric aerosols.

2. Since Mars is located near the asteroid belt and also since photographs of its surface by Mariners 4, 6, and 7 show what appears to be evidence of extensive meteoritic bombardment, meteoric particles may be a source of Martian atmospheric aerosols. The minerals which are present in most common meteorites have a refractive index of the order of 1.65, a value which falls within the range of refractive indices for which the above calculations exhibit an opposition effect.

3. Measurements of the dielectric constant of the Martian surface indicate that the abundance of limonite in the surface material is relatively low (Beck et al, 1969). Comparison with terrestrial and lunar abundances indicates that the mineral species to be expected in the Martian surface material are feldspar, pyroxene, olivine, amphibole, quartz, magnetite, ilmenite, hematite, and limonite (goethite) (Beck et al, 1969; P.D. Lowman, Jr., private communication). Table IV lists typical refractive indices for these minerals (Wahlstrom, 1947). The last four are highly absorbing and could not, therefore, exhibit an opposition effect, as the above light scattering calculations for limonite show. The more transparent minerals in Table IV, on the other hand, do have indices of refraction in the range where it has been demonstrated that an opposition effect is obtained. If submicron

Table IV. Refractive Indices of Minerals Expected to be Present on Mars

Mineral Group	Typical Composition	Refractive Index
Feldspar	$CaAl_2Si_2O_8$; $NaAlSi_3O_8$; $KAlSi_3O_8$	1.52—1.59
Pyroxene	$Ca(Mg,Fe,Al)(Si,Al)_2O_6$; $MgSiO_3$	1.65—1.75
Olivine	$(Mg,Fe)_2SiO_4$	1.65—1.88
Amphibole	$Ca_2(Mg,Fe)_5Si_8O_{22}(OH)_2$	1.60—1.67
Quartz	SiO_2	1.54—1.55
Magnetite	Fe_3O_4	*
Ilmenite	$FeTiO_3$	*
Hematite	Fe_2O_3	~ 3.0*
Limonite (Goethite)	$HFeO_2$	>2.0

* opaque

dust particles of such rock-forming minerals were swept up from the Martian surface and suspended in its atmosphere, the calculations suggest that the observed opposition effect could be produced. The complex index of refraction of a basaltic rock was measured by Egan and Becker (1969) and found to be $1.65 - 0.01i$ between wavelengths of 0.35μ and 1.0μ. Such a material would satisfy the requirements for the dust particles in the Martian atmosphere. Indeed, a basaltic-type surface composition has been predicted for Mars (Beck et al, 1969).

Because the Martian atmospheric density is very low, one might question whether the atmosphere could support aerosols. It is interesting to note in this regard that in the earth's stratosphere, where the density is roughly comparable to that near the surface of Mars, there exists a worldwide permanent layer of submicron aerosol particles, containing sulfur as a major constituent, with traces of iron and silicon (Junge et al, 1961).

VI. Summary and Conclusions

The Mie theory was used to compute the light scattered by spherical aerosol particles suspended in the Martian atmosphere to determine if atmospheric aerosols can produce the observed Martian opposition effect. This effect is more pronounced in the ultraviolet than in the infrared.

First, the scattering by individual submicron particles of refractive indices $\underline{n}$ ranging from 1.20 to 2.40 was examined to see which indices show a significant increase in brightness at phase angles $\lesssim 10^{\circ}$. Neither indices of 1.50 or less, which include ice, water, and solid CO_2, nor highly absorbing indices, such as that for limonite, gave results characteristic of the opposition effect. Indices of 1.55 and greater with little or no absorption, on the other hand, did show increased reflectivity at small phase angles with insignificant contributions at larger phase angles.

Next, we applied several submicron particle size distributions to the scattering by individual particles in order to obtain integrated intensities. As anticipated from the calculations for individual particles, these integrated intensities also showed that only refractive indices greater than 1.50 exhibit a definite increase in brightness at small phase angles without significant enhancements at larger phase angles.

The third step was to generate a model consisting of a surface photometric function plus an aerosol brightness contribution. The

surface function was chosen to have the same shape at all wavelengths; only the albedo differed, according to the observed wavelength-dependence of the Martian albedo observations.

Models having aerosols with $\underline{n} = 1.55$ and 1.75 both fit reasonably well with the observational data: the aerosol brightness contribution provided a significant enhancement at small phase angles in the ultraviolet, where the albedo is low, and yet at the same time made a negligible contribution in the infrared, where the surface albedo is high. A similar fit would probably be obtained with any real index between 1.55 and 1.75.

Although the fitting of the model was somewhat arbitrary and by no means a unique solution to the problem, it did show that the observed opposition effect can be produced by atmospheric aerosols with the proper index of refraction. In this model, a columnar density of 0.9×10^6 aerosols/cm^2 with average particle radius of 0.4μ gave the required aerosol contribution to the total reflectivity. Assuming a density of 2.5 gm/cm^3, this corresponds to a mass ratio of aerosols to gaseous atmosphere (for a Martian surface pressure of 7 mb) of 4×10^{-8}. This indicates that only a very small amount of aerosols is needed to produce the observed opposition effect.

Finally, a number of possible sources of planetary atmospheric aerosols were considered: <u>in situ</u> particle formation from gaseous atmospheric constituents; influx of meteoric particles; and upsweeping of dust from the surface of the planet. Refractive indices of repre-

sentative substances in each group were discussed. The most promising candidates are semi-transparent minerals, most of which have n between 1.55 and 1.75. This suggests that meteoric particles from outside the planet or dust from the surface of the planet may be present as atmospheric aerosols, thus producing the Martian opposition effect.

ACKNOWLEDGMENTS

I thank Dr. Paul D. Lowman, Jr., for patiently introducing me to the nomenclature of mineralogy and for his helpful discussions regarding the surface of Mars. I am also grateful to Drs. Louis S. Walter and John A. O'Keefe for their useful comments.

REFERENCES

Beck, A. J., and de Wys, E. C. (1969). Mars surface models (1968). NASA (Natl. Aeron. Space Admin.) SP-8020.

de Vaucouleurs, G. (1964). Geometric and photometric parameters of the terrestrial planets. Icarus 3, 187-235.

de Vaucouleurs, G. (1968). On the opposition effect of Mars. Icarus 9, 598-599.

Egan, W. G., and Becker, J. F. (1969). Determination of the complex index of refraction of rocks and minerals. Appl. Opt. 8, 720-721.

Egan, W. G., and Spagnolo, F. A. (1969). Complex index of refraction of bulk solid carbon dioxide. Appl. Opt. 8, 2359-2360.

Hapke, B. W. (1963). A theoretical photometric function for the lunar surface. J. Geophys. Res. 68, 4571-4586.

Junge, C. E., Chagnon, C. W., and Manson, J. E. (1961). Stratospheric aerosols. J. Meteorol. 18, 81-108.

Kliore, A., Fjeldbo, G. Seidel, B. L., and Rasool, S. I. (1969). Mariners 6 and 7: radio occultation measurements of the atmosphere of Mars. Science 166, 1393-1397.

O'Leary, B. T. (1967a). The opposition effect of Mars. Astrophys. J. 149, L147-L149.

REFERENCES (Cont.)

O'Leary, B. T. (1967b). Mars: visible and near infrared studies and the composition of the surface, Ph.D. Thesis, University of California, Berkeley, 165 pp.

O'Leary, B. T., and Rea, D. G. (1968). The opposition effect of Mars and its implications. Icarus 9, 405-428.

Tempelmeyer, K. E., and Mills, E. W., Jr. (1968). Refractive index of carbon dioxide cryodeposit. J. Appl. Phys. 39, 2968-2969.

van de Hulst, H. C. (1957). "Light Scattering by Small Particles". Wiley, New York.

Wahlstrom, E. E. (1947). "Igneous Minerals and Rocks". Wiley, New York.